DEUTSCHES ELEKTRONEN – SYNCHROTRON

DESY 92-160
November 1992

Total Photoproduction Cross Section Measurement at HERA Energies

H1 Collaboration

ISSN 0418-9833

NOTKESTRASSE 85 · D-2000 HAMBURG 52

To be sure that your preprints are promptly included in the
HIGH ENERGY PHYSICS INDEX,
send them to (if possible by air mail):

DESY Bibliothek Notkestraße 85 W-2000 Hamburg 52 Germany	DESY-IfH Bibliothek Platanenallee 6 O-1615 Zeuthen Germany

DESY 92-160
November 1992

ISSN 0418-9833

Total Photoproduction Cross Section Measurement at HERA Energies

H1 Collaboration

T. Ahmed[3], V. Andreev[22], B. Andrieu[25], M. Arpagaus[32], A. Babayev[21], H. Bärwolff[31], J. Ban[16], P. Baranov[22], E. Barrelet[26], W. Bartel[11], U. Bassler[26], G.A. Beck[17], H.P. Beck[33], H.-J.Behrend[11], A. Belousov[22], Ch. Berger[1], H. Bergstein[1], G. Bernardi[26], R. Bernet[32], G. Bertrand-Coremans[4], M. Besançon[9], P. Biddulph[20], E. Binder[11], J.C. Bizot[24], V. Blobel[13], K. Borras[8], P.C. Bosetti[2], V. Boudry[25], C. Bourdarios[24], F. Brasse[11], U. Braun[2], W. Braunschweig[1], V. Brisson[24], D. Bruncko[15], J. Bürger[11], F.W. Büsser[13], A. Buniatian[11,35], S. Burke[17], G. Buschhorn[23], A.J. Campbell[10], T. Carli[25], F. Charles[26], D. Clarke[5], A.B. Clegg[16], M. Colombo[8], J.A. Coughlan[5], A. Courau[24], Ch. Coutures[9], G. Cozzika[9], L. Criegee[11], J. Cvach[25], J.B. Dainton[17], M. Danilov[21], A.W.E. Dann[20], W.D. Dau[14], M. David[9], E. Deffur[11], B. Delcourt[24], L. DelBuono[26], M. Devel[24], A. DeRoeck[11], P. Dingus[25], C. Dollfus[33], J.D. Dowell[3], H B. Dreis[2], A. Drescher[8], J. Duboc[26], D. Düllmann[13], O. Dünger[13], H. Duhm[12], M. Eberle[12], J. Ebert[30], T.R. Ebert[17], G. Eckerlin[11], V. Efremenko[21], S. Egli[33], S. Eichenberger[33], R. Eichler[32], F. Eisele[11], E. Eisenhandler[18] N.N. Ellis[3], R.J. Ellison[20], E. Elsen[11], M. Erdmann[11], E. Evrard[4], L. Favart[4], A. Fedotov[21], D. Feeken[13], R. Felst[11], J. Feltesse[9], Y. Feng[26], I.F. Fensome[3], J. Ferencei[11], F. Ferrarotto[29], W. Flauger[11,l], M. Fleischer[11], G. Flügge[2], A. Fomenko[22], B. Fominykh[21], M. Forbush[7], J. Formanek[28], J.M. Foster[20], G. Franke[11], E. Fretwurst[12], P. Fuhrmann[1], E. Gabathuler[17], K. Gamerdinger[23], J. Garvey[3], J. Gayler[11], A. Gellrich[13], M. Gennis[11], U. Gensch[31], H. Genzel[1], R. Gerhards[11], D. Gillespie[17], L. Godfrey[7], U. Goerlach[11], L. Goerlich[6], M. Goldberg[26], A.M. Goodall[17], I. Gorelov[21], P. Goritchev[21], C. Grab[32], H. Grässler[2], R. Grässler[2], T. Greenshaw[17], H. Greif[23], G. Grindhammer[23], C. Gruber[14], J. Haack[31], D. Haidt[11], L. Hajduk[6], O. Hamon[26], D. Handschuh[11], E.M. Hanlon[16], M. Hapke[11], J. Harjes[13], P. Hartz[8], R. Haydar[24], W.J. Haynes[5], J. Heatherington[18], V. Hedberg[19], R. Hedgecock[5], G. Heinzelmann[13], R.C.W. Henderson[16], H. Henschel[31], R. Herma[1], I. Herynek[27], W. Hildesheim[26], P. Hill[11], C.D. Hilton[20], J. Hladky[27], K.C. Hoeger[20], Ph. Huet[4], H. Hufnagel[8], N. Huot[26], M. Ibbotson[20], M.A. Jabiol[9], A. Jacholkowska[24], C. Jacobsson[19], M. Jaffre[24], L. Jönsson[19], K. Johannsen[13], D.P. Johnson[4], L. Johnson[16], H. Jung[2], P.I.P. Kalmus[18] S. Kasarian[11], R. Kaschowitz[2], P. Kasselmann[12], U. Kathage[14], H. H.Kaufmann[31], I.R. Kenyon[3], S. Kermiche[24], C. Kiesling[23], M. Klein[31], C. Kleinwort[13], G. Knies[11], T. Köhler[1], H. Kolanoski[8], F. Kole[7], S.D. Kolya[20], V. Korbel[11], M. Korn[8], P. Kostka[31], S.K. Kotelnikov[22], M.W. Krasny[6,9], H. Krehbiel[11], D. Krücker[2], U. Krüger[11], J.P. Kubenka[23], H. Küster[11], M. Kuhlen[23], T. Kurca[16], J. Kurzhöfer[8], B. Kuznik[30], R. Lander[7], M.P.J. Landon[18] R. Langkau[12], P. Lanius[23], J.F. Laporte[9], A. Lebedev[22], A. Leuschner[11], C. Leverenz[11], D. Levin[11], S. Levonian[11,22], Ch. Ley[2], A. Lindner[8], G. Lindström[12], P. Loch[13], H. Lohmander[19], G.C. Lopez[18], D. Lüers[23,l], N. Magnussen[30], E. Malinovski[22], S. Mani[7], P. Marage[4], J. Marks[10], R. Marshall[20], J. Martens[30], R. Martin[17], H.-U. Martyn[1], J. Martyniak[8], S. Masson[2], A. Mavroidis[18] S.J. Maxfield[17], S.J. McMahon[17], A. Mehta[20], K. Meier[11], T. Merz[11], C.A. Meyer[33], H. Meyer[30], J. Meyer[11], S. Mikocki[6,24], V. Milone[29], E. Monnier[26], F. Moreau[25], J. Moreels[4], J.V. Morris[5], J.M. Morton[17],

K. Müller[33], P. Murin[15], S.A. Murray[20], V. Nagovizin[21], B. Naroska[13], Th. Naumann D. Newton[16], H.K. Nguyen[26], F. Niebergall[13], R. Nisius[1], G. Nowak[6], G.W. Noyes[3], M. Nyberg[19], H. Oberlack[23], U. Obrock[8], J.E. Olsson[11], S. Orenstein[25], F. Ould-Saa C. Pascaud[24], G.D. Patel[17], E. Peppel[11], S. Peters[23], H.T. Phillips[3], J.P. Phillips[20], Ch. Pichler[12], W. Pilgram[2], D. Pitzl[32], R. Prosi[11], F. Raupach[1], K. Rauschnabel[8], P. Reimer[27], P. Ribarics[23], V. Riech[12], J. Riedlberger[32], M. Rietz[2], S.M. Robertson[3], P. Robmann[33], R. Roosen[4], A. Rostovtsev[21], C .Royon[9], M. Rudowicz[23], M. Ruffer[12] S. Rusakov[22], K. Rybicki[6], E. Ryseck[31], J. Sacton[4], N. Sahlmann[2], E. Sanchez[23], D.P. Sankey[5], M. Savitsky[11], P. Schacht[23], P. Schleper[1], W. von Schlippe[18], C. Schmi D. Schmidt[30] W. Schmitz[2], V. Schröder[11], M. Schulz[11], A. Schwind[31], W. Scobel[12], U. Seehausen[13], R. Sell[11], M. Seman[15], A. Semenov[21], V. Shekelyan[21], I. Sheviakov[22] H. Shooshtari[29], G. Siegmon[14], U. Siewert[14], Y. Sirois[25], I.O. Skillicorn[10], P. Smirnov J.R. Smith[7], L. Smolik[11], Y. Soloviev[22], H. Spitzer[13], P. Staroba[27], M. Steenbock[13], P. Steffen[11], R. Steinberg[2], H. Steiner[26], B. Stella[29], K. Stephens[20], J. Stier[11], J. Stra U. Straumann[33], W. Struczinski[2], J.P. Sutton[20], R.E. Taylor[34,24], G. Thompson[18] R.J.Thompson[20], I. Tichomirov[21], C. Trenkel[14], P. Truöl[33], V. Tchernyshov[21], J. Turi J. Tutas[1], L. Urban[23], A. Usik[22], S. Valkar[28], A. Valkarova[28], C. Vallee[26], P. VanEsch Vartapetian[11,35], Y. Vazdik[22], M. Vecko[27], P. Verrecchia[9], R. Vick[13], G .Villet[9], E. Vo K. Wacker[8], I.W. Walker[16], A. Walther[8], G. Weber[13], D. Wegener[8], A. Wegner[11], H. P.Wellisch[23], S. Willard[7], M. Winde[31], G.-G. Winter[11], Th. Wolff[32], L.A. Womersl A.E. Wright[20], N. Wulff[11], T.P. Yiou[26], J. Zacek[24,28], P. Zavada[27], C. Zeitnitz[12], H. Ziaeepour[24], M. Zimmer[11], W. Zimmermann[11], and F. Zomer[24]

[1] *I. Physikalisches Institut der RWTH, Aachen , Germany[a]*
[2] *III. Physikalisches Institut der RWTH, Aachen , Germany[a]*
[3] *School of Physics and Space Research, University of Birmingham, Birmingham, UK[b]*
[4] *Inter-University Institute for High Energies ULB-VUB, Brussels, Belgium*
[5] *Rutherford Appleton Laboratory, Chilton, Didcot, UK[b]*
[6] *Institute for Nuclear Physics, Cracow, Poland*
[7] *Physics Department and IIRPA, University of California, Davis, California, USA[c]*
[8] *Institut für Physik, Universität Dortmund, Dortmund, Germany[a]*
[9] *DAPNIA, Centre d'Etudes de Saclay, Gif-sur-Yvette, France*
[10] *Department of Physics and Astronomy, University of Glasgow, Glasgow, UK[b]*
[11] *DESY, Hamburg, Germany[a]*
[12] *I. Institut für Experimentalphysik, Universität Hamburg, Hamburg, Germany[a]*
[13] *II. Institut für Experimentalphysik, Universität Hamburg, Hamburg, Germany[a]*
[14] *Institut f. Reine und Angewandte Kernphysik, Universität Kiel , Germany[a]*
[15] *Institute of Experimental Physics, Slovak Academy of Sciences, Kosice , CSFR*
[16] *School of Physics and Materials, University of Lancaster, Lancaster, UK[b]*
[17] *Department of Physics, University of Liverpool, Liverpool, UK[b]*
[18] *Queen Mary and Westfield College, London, UK[b]*
[19] *Physics Department, University of Lund, Lund, Sweden[d]*
[20] *Physics Department, University of Manchester, Manchester, UK[b]*
[21] *Institute for Theoretical and Experimental Physics, Moscow, Russia*
[22] *Lebedev Physical Institute, Moscow, Russia*
[23] *Max-Planck-Institut für Physik, München, Germany[a]*
[24] *LAL, Université de Paris-Sud, IN2P3-CNRS, Orsay, France*
[25] *LPNHE, Ecole Polytechnique, IN2P3-CNRS, Palaiseau, France*
[26] *LPNHE, Universités Paris VI and VII, IN2P3-CNRS, Paris, France*
[27] *Institute of Physics, Czechoslovak Academy of Sciences, Praha, CSFR*

[28] *Nuclear Center, Charles University, Praha, CSFR*
[29] *INFN Roma and Dipartimento di Fisica, Universita "La Sapienzia", Roma, Italy*
[30] *Fachbereich Physik, Bergische Universität Gesamthochschule Wuppertal, Wuppertal, Germany*[a]
[31] *DESY, Institut für Hochenergiephysik, Zeuthen, Germany*[a]
[32] *Institut für Mittelenergiephysik, ETH, Zürich, Switzerland*[e]
[33] *Physik-Institut der Universität Zürich, Zürich, Switzerland*[e]
[34] *Stanford Linear Accelerator Center, Stanford Californa, USA*
[35] *Visitor from Yerevan Phys.Inst., Armenia*
† *Deceased*

[a] *Supported by the Bundesministerium für Forschung und Technologie, FRG*
[b] *Supported by the UK Science and Engineering Research Council*
[c] *Supported in part by USDOE grant DE F603 91ER40674*
[d] *Supported by the Swedish Natural Science Research Council*
[e] *Supported by the Swiss National Science Foundation*

Abstract

We present first results on the total photoproduction cross section measurement with the H1 detector at HERA. The data were extracted from low Q^2 collisions of 26.7 GeV electrons with 820 GeV protons. The γp total cross section has been measured by two independent methods in the γp center of mass energy range from 90 to 290 GeV. For an average center of mass energy of 195 GeV a value of $\sigma_{tot}(\gamma p) = 159 \pm 7(stat.) \pm 20(syst.)$ μb was obtained.

Submitted to Physics Letters B, 17 November 1992

1 Introduction

The total cross section is an important quantity strongly related to the fund properties of particle interactions and to the structure of the interacting parti particular, various theoretical models are quite sensitive to the high-energy beha the photon-proton total cross section, predicting for $\sigma_{tot}(\gamma p)$ values between 145 760 μb at 250 GeV center of mass energy [1]. This uncertainty reflects the lim in our present knowledge of both the proton and photon structure at high ener

Since the previous experimental data [2] were limited to center of mass less than 18 GeV they allowed for different energy dependencies of $\sigma_{tot}(\gamma p)$. H new electron-proton collider HERA offers a unique possibility to measure the cross section up to the center of mass energy of $\sim$ 300 GeV and to reduce the uncertainty.

In this paper a measurement of $\sigma_{tot}(\gamma p)$ in the center of mass energy range 90 and 290 GeV, performed with the H1 detector, is presented. The data for the were collected during the first running period of the ep collider HERA in July 1 correspond to a total integrated luminosity of 1.5 nb^{-1}. Preliminary results study were presented in [3]. Recently another measurement of $\sigma_{tot}(\gamma p)$ at HE been published in [4].

2 The Method

The γp cross section measurement at HERA is based on the low Q^2 ep-scattering In the single photon exchange approximation the ep cross section at fixed center energy can be written as

$$\frac{d^2\sigma_{ep}}{dydQ^2} = \frac{\alpha}{2\pi}\frac{1}{Q^2}\left\{B(y,Q^2)\sigma_T(y,Q^2) + C(y,Q^2)\sigma_L(y,Q^2)\right\}$$

where $Q^2 = -q^2$ is the virtuality of the photon and, for small scattering angl $1 - E'_e/E_e$. E_e and E'_e are the energies of the initial and the scattered electron, B and $C(y,Q^2)$ are kinematical factors, and σ_T and σ_L are the cross sections for tra and longitudinally polarized virtual photons respectively. For very small Q^2 use the Weizsäcker-Williams approximation (WWA) [5] to simplify (1) after inte over the Q^2 dependence:

$$\frac{d\sigma_{ep}}{dy} = \sigma_{tot}(W_{\gamma p})Flux(y) = \sigma_{tot}(W_{\gamma p})\frac{\alpha}{2\pi}\frac{1+(1-y)^2}{y}\ln\frac{Q^2_{max}(y)}{Q^2_{min}(y)}$$

with $W_{\gamma p} = \sqrt{s_{\gamma p}} = 2\sqrt{yE_eE_p}$ and $Q^2_{min}(y) = (m_e y)^2/(1-y)$. The value of Q^2_m defined by the actual experimental conditions.

In general, two different methods are possible to study photoproduction with detector:

- use only tagged events, in which the energy of small angle scattered e ($\theta_{e'} < 5$ mrad with respect to the electron beam direction) is measured in electron tagger, or

- use all events in which electrons are scattered by angles $\theta_{e'} < 70$ mrad. These electrons cannot be detected by the main H1 detector and escape in the beampipe (non-tagged events).

These methods access different but overlapping kinematical domains and are explored by different triggers, thus allowing for a complementary view on photoproduction events. For tagged events the acceptance of the H1 apparatus is limited to the range [6]

$$0.2 < y < 0.8, \quad 3 \cdot 10^{-8}\ \mathrm{GeV}^2 < Q^2 < 10^{-2}\ \mathrm{GeV}^2.$$

For this small Q^2, equation (2) deviates from (1) by less than 0.3% [7]. Another important advantage of using tagged events is the possibility to measure y with good precision and thus to know the actual value of $W_{\gamma p}$ within the range 150 GeV$< W_{\gamma p} <$ 250 GeV. On the other hand the non-tagged event sample has about a 10 times larger acceptance and covers a wider energy interval 90 GeV$< W_{\gamma p} <$ 290 GeV although the y-resolution, based on the hadron energy flow measurement [9], is poor. Moreover, in this approach Q^2_{max} is ≈ 4 GeV^2 and therefore corrections to the WWA of the order of 10 to 15% must be taken into account [7,8].

To summarize, we used tagged events as the basic and most precise method for the measurement of the total cross section and non-tagged events as an independent check of the measurement.

3 Experimental Setup

Presently the HERA accelerator collides 26.7 GeV electrons with 820 GeV protons. The particles are grouped in bunches separated by 96 ns time intervals. In the first running period in July 1992 usually 10 proton and 10 electron bunches were injected into the machine. Only 9 bunches were made to collide while one bunch per beam was used to check the background. The currents, typically of 100 to 200 μA per bunch, were measured for each bunch separately with a precision of $\approx 1\%$. The detectors H1 and ZEUS recorded the collision products at two interaction regions in the north and the south straight sections of the HERA ring, respectively. The size of the interaction region, determined by the lengths of the proton bunches, covered a range of ± 50 cm around the nominal interaction point.

A description of the H1 detector can be found elsewhere [10]. Here we emphasize only those detector parts relevant to the total cross section measurement. The H1 detector is asymmetric with respect to the interaction point since the events are boosted in the proton (forward,+z) direction leading there to high particle energies and densities. Consequently the tracking system of the detector is split into a central part covering polar angles between 20 and 160 degrees and a forward part for particles between 7 and 25 degrees. Magnetic bending is provided by a superconducting solenoid with a radius of 3 m which produces a homogenous field of 1.14 T along the z axis. The interaction region is surrounded by a system of cylindrical driftchambers with two jet chambers and two z chambers. Resolutions of $\sigma_{r\phi} = 200$ μm for the jet chambers and $\sigma_z = 250$ μm for the z chambers have been achieved. The mean resolution for dE/dx measurements

in the jet chambers is 12%. The driftchambers are interleaved by an inner
an outer (COP) double layer of cylindrical multiwire proportional chambers
readout at radii of 16 cm and 51 cm. These are used for the first level trigge
on charged tracks coming from the interaction region. The backward trackin
covered by a multiwire proportional chamber with four wire planes. It prov
points for tracks with polar angles between 154 and 176 degrees.

The tracking area is surrounded by a fine grain liquid argon calorimeter co
the electromagnetic and hadronic sections. It covers polar angles between 4°
The energy resolutions are $\sigma(E)/E = 0.12/\sqrt{E}$ for electrons and $\sigma(E)/E =$
for hadrons with E in GeV. In the backward region the detector is compl
lead-scintillator sandwich calorimeter with an energy resolution of $\sigma(E)/E =$
for electrons. A time of flight counter system (TOF) behind this calorimeter
veto against proton beam initiated background from upstream.

A luminosity system measuring the reaction $ep \to e\gamma p$ is located in the
direction with an "electron tagger" at $z = -33$ m and a photon detector at $z =$
Each component consists of a $TlCl/TlBr$ crystal calorimeter having an energy
of $\sigma(E)/E = 0.1/\sqrt{E}$ and space resolution of $\sigma(x,y) = 0.2$ cm. The electr
accepts electrons with energies E'_e in the range $0.2E_e < E'_e < 0.8E_e$ and po
below 5 mrad. The geometrical acceptance of the photon detector for brems
photons is $\sim 98\%$. The system has two independent electronics branches wh
to measure luminosity and to trigger on photoproduction candidates simulta

4 Trigger and Event Selection

At HERA the ep signal has to compete with the strong background from pr
collisions and beam–wall events. Hence the number of triggers recorded by t
ment is large (about 3,000,000 in this first luminosity period) while the expecte
of photoproduction events amounts to a few thousand only. The data for thi
were taken in July 1992. The typical luminosity amounted to 40 mb^{-1}s^{-1}
total integrated luminosity of 1.5 nb^{-1}. A set of dedicated triggers for photop
events was included in the H1 trigger system which allowed continuous data
both tagged and non-tagged events throughout the whole run period simul
with triggers for other event classes. For tagged events the following trigger
was imposed:

- Energy in the electron tagger calorimeter $E'_e > 4$ GeV and energy in th
calorimeter $E_\gamma < 2$ GeV.
- At least one "ray" found in the central tracking detector.

The requirement $E_\gamma < 2$ GeV was necessary to reduce the high background
bremsstrahlung events $ep \to e\gamma p$ having a typical rate of a few kHz. A "ray" wa
as a coincidence of 2 pads from the CIP and 2 pads from the COP, such that
line in the r-z plane through all four pads intercepted the z axis within ± 44
nominal interaction point [11]. The requirement on E'_e reduced the trigger ra

orders of magnitude [6] leading to an acceptable trigger rate of 0.1 Hz. For non-tagged events this suppression factor must come from a stronger requirement on the charged track multiplicity of the event. Therefore at least three rays were demanded. The z coordinate of the intercept of all rays with the z axis was added to a 16 bin wide z-vertex histogram. The event was triggered if the content of the peak bin was significantly above the mean content of all other bins and if the peak position was within ± 33 cm. Both triggers were disabled if the signals from the TOF detector arrived in a time window expected from upstream proton induced background.

In a first step of the offline analysis some obvious sources of background events such as proton interactions in the beampipe and cosmic ray events were removed. Background events induced by electrons were almost completely suppressed by requiring at least one reconstructed track in the central tracker with a transverse momentum above 100 MeV/c. The dominant source of background events after these selections were interactions of protons with the residual gas within the H1 detector. For the tagged events they appeared in random coincidence with a signal in the electron tagger. The energy flow of these events was characterized by a value of $\sum p_z / \sum p$ near to 1, due to the large Lorentz boost, and a small value for $y_h = \sum (E - p_z) / 2E_e$. The summation was performed over tracks and calorimeter cells, where calorimeter cells behind tracks were masked to avoid double counting of energy. Figure 1 shows the event distribution in the two variables for a background sample taken from events coming from the so called proton pilot bunch with no electron bunch partner compared to the photoproduction

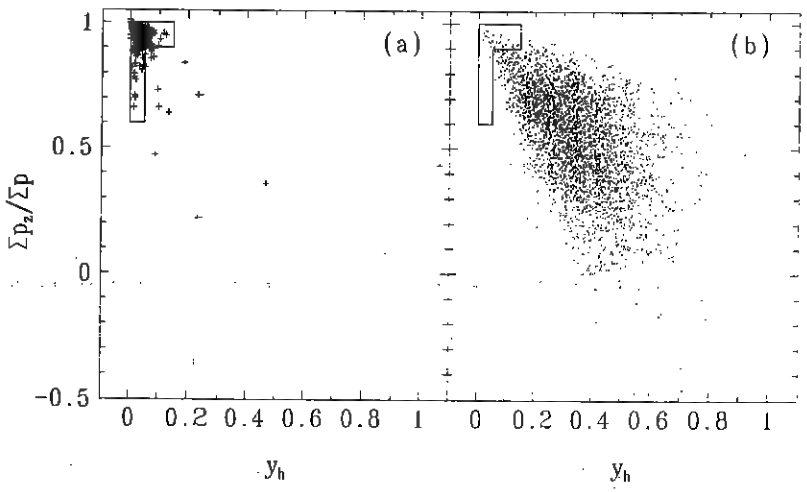

Figure 1: Distributions of $\sum p_z / \sum p$ versus y_h for the proton pilot bunch data (a) and for tagged γp MC events (b). The cuts applied for the proton−gas background rejection are indicated by the solid line.

events from Monte Carlo simulation (see section 5). Also the applied cuts a
cated. These background events are often accompanied by a number of proton
are identified by their energy loss in the central jet chamber. Thus events in w
reconstructed tracks were identified as protons and events with 3 or more proto
also rejected.

A total of 1383 tagged and 9073 non-tagged events survived the offline se
The remaining background events were statistically subtracted from both data s
For the tagged events the shape of the measured E'_e spectrum has been used
purpose. As shown in Figure 2a the spectrum consists of two parts, one part
photoproduction events with a peak at about 15 GeV and another part with a c
shape giving rise to a peak around 20 GeV. The shape of this background sp
was monitored throughout the whole run period by a downscaled pure electron
trigger. As an independent cross check the events from the non-colliding electron
were used to define the background at the electron tagger. Both background
agree well and give the same final result.

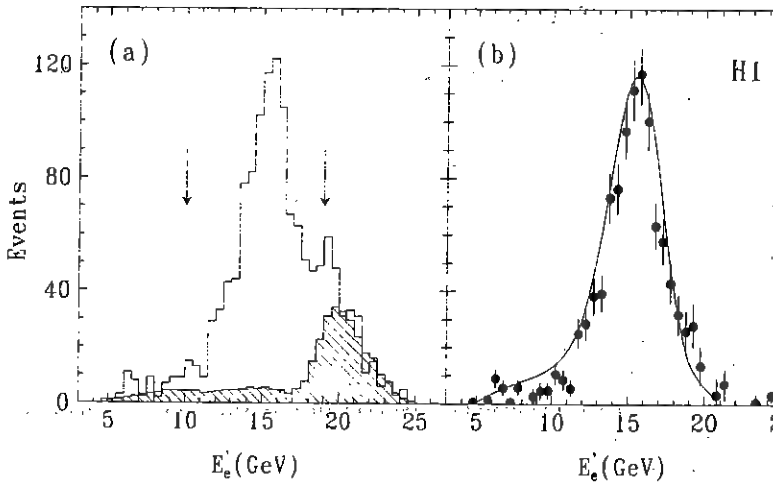

Figure 2: Energy distributions of the tagged scattered electrons. In (a) the holl
togram is for the full tagged sample and the hatched histogram denotes the norr
background spectrum. After statistical subtraction of the background the data (
are compared to the Monte Carlo calculation (curve) taking into account the me
beam conditions (b). The arrows in (a) indicate the energy region used for t
measurement.

The background peak was normalized to the measured distribution taking the part of the spectrum above 20 GeV. After the statistical subtraction the shape of the E'_e spectrum (Figure 2b) agrees well with the Monte Carlo calculation taking into account electron beam tilts in the horizontal and vertical planes of the order of 0.1 mrad, measured by the photon detector of the H1 luminosity system. In order to remove the tails of the distribution where the electron tagger acceptance is small, only the events from the energy interval between 10 GeV and 19 GeV have been used for the final analysis. The cuts were motivated by a compromise between the sensitivity to the absolute energy calibration of the tagger ($\sim$ 3%) and the signal to background ratio (10 to 1 in the chosen energy range). Four events in the electron pilot bunch survived all selections and gave an estimate of the non-random background from the γA photoproduction on the residual gas. After scaling up with the ratio of the electron current in the colliding bunches to the pilot bunch current this background was found to be (4.2 ± 2.1)% and has been subtracted from the final sample as well.

For the non-tagged events the statistical background subtraction was done by exploiting the so called "empty target" method using the proton and electron pilot bunches in which there is no colliding partner. Taking into account the measured currents for each of the bunches the number of photo-produced events can be derived from the total number of events by the formula

$$N_{\gamma p} = N_{total} - \sum_i R_i^p \times N_i^{p-pilot} - \sum_i R_i^e \times N_i^{e-pilot}$$

Here R_i^p and R_i^e denote the ratios of the total beam current to the pilot bunch current for a given run i and $N_i^{p-pilot}$ and $N_i^{e-pilot}$ are the number of observed events in the pilot bunches. Figure 3a shows that the bulk of the background is concentrated at small values of y_h. The resulting y_h-distribution shown in Figure 3b demonstrates good agreement with the ep Monte Carlo simulated events passing the same selection criteria. To minimize the statistical error for this sample only the region of $0.15 < y_h < 1.0$ has been used where the signal to background ratio is 2.41. This cut selects γp events with an average center of mass energy $W_{\gamma p} = 183$ GeV, compared to the average $W_{\gamma p} = 195$ GeV for the tagged sample.

The quality of the event selection can be checked with the vertex distributions along the z axis. It was found, that the distributions for both tagged and non-tagged samples have approximately gaussian shape with $\sigma_z \approx 14$ cm, in contrast to the expected flat shape for the background events.

The final number of photoproduction events is 917 ± 38 for the tagged sample and 940 ± 65 for the non-tagged sample where the errors are the statistical errors of the subtraction method. An overlapping part of the two samples contains 170 events satisfying both trigger conditions and all offline selections.

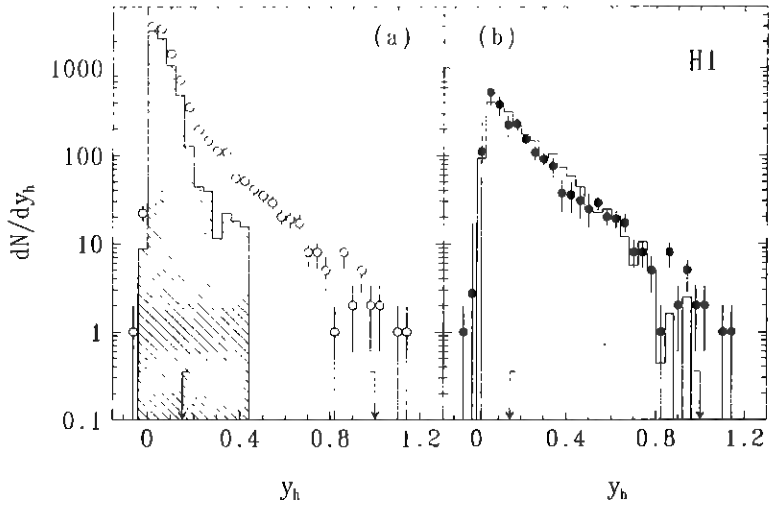

Figure 3: y_h-distribution for the non-tagged events. The arrows indicate the ar for the final analysis. (a) The points describe the distribution for the full sam the hatched histogram is the distribution for the pilot bunch events normalized total current (an average normalization factor $< R^p >= 8.1$). (b) After statistic traction of the background the data (points) are compared to Monte Carlo simu (histogram).

5 Acceptance Studies

One of the important aspects of this analysis is the determination of the detec ceptance. Here we define the acceptance as a function which takes into acco geometrical acceptance, the trigger efficiency and the event selection efficiency the acceptance of the electron tagger depends only on the parameters of the sc electron and not on the details of the photoproduction process, its calculation is simple. Therefore we concentrate on the study of the main detector acceptance.

The total cross section can be decomposed into a set of different subprocesse

$$\sigma_{tot} = \sigma_D + \sigma_{ND} = \sigma_{el} + \sigma_{sd} + \sigma_{dd} + \sigma_{ND}^{soft} + \sigma_{ND}^{hard}$$

The diffractive component σ_D contains contributions from the 'elastic' scatterin $\rho^0 p$, single diffractive dissociation $\gamma p \to \rho^0 M_x$ and $\gamma p \to M_x p$ and double diff dissociation $\gamma p \to M_{x1} M_{x2}$. The channel $\gamma p \to \gamma p$ contributes only 10% to th elastic γp scattering [12] and therefore can be neglected. The non-diffractive p be split into the 'soft' and 'hard' scattering processes.

The 'soft' processes were generated according to the vector-meson dominance model using the RAYPHOTON generator [13] in a low p_T mode. For the 'hard' scattering events the PYTHIA 5.6 [14] was used to generate the photon interactions with the partons inside the proton. PYTHIA has also been adapted to generate the elastic and diffractive photoproduction events according to the distribution $\frac{d\sigma}{dt} \sim e^{-b|t|}$ with $b_{sd} = \frac{1}{2} b_{el}$. In the elastic channel helicity conservation was required for the ρ^0 decay.

The various subprocesses have different acceptances which are themselves functions of the photon energy. Therefore one has to make some *a priori* assumption about the relative contribution of the subprocesses in order to translate the total number of observed events to the cross section. To make a realistic ansatz concerning the diffractive component, the measured properties of γp events at low energies [12] were extrapolated to the HERA domain using the energy dependencies known from hadron−hadron collisions [15]. All errors involved were propagated as well. The mean values for the relative contribution of 'soft' and 'hard' components to the total γp cross section were determined by comparing various experimental distributions of the tagged events with those from the Monte Carlo events. The best description of the data was obtained for the following set:

$$\frac{\sigma_D}{\sigma_{tot}} = 0.26; \quad \frac{\sigma_{ND}^{soft}}{\sigma_{tot}} = 0.55; \quad \frac{\sigma_{ND}^{hard}}{\sigma_{tot}} = 0.19 \qquad (3)$$

For example, the inclusive charged particle distributions shown in Figure 4 demonstrate a good agreement between our data and the Monte Carlo simulation using the composition (3), whereas an ansatz e.g. without 'hard' component cannot describe the data correctly. The assumption about the contribution of the diffractive part is in agreement with the observed $(6.3 \pm 1.9)\%$ of the tagged events with no energy deposition in the forward calorimeter ($\theta < 25°$). To arrive at a conservative estimate of a systematic error in the acceptance determination due to the uncertainty in the decomposition (3) we varied the relative contribution of the subprocesses within the following limits: 0.26 ± 0.06, 0.55 ± 0.15, 0.19 ± 0.15.

The acceptance of the trigger and event selection for photoproduction events was derived from the Monte Carlo simulations. For the simulations the performance of the detector, in particular its trigger efficiency and acceptance was tuned to the trigger efficiencies as measured in the data. As an example, the efficiencies for giving a "ray" trigger as a function of the track parameters like transverse momentum, polar and azimuthal angle and z position were determined from the data. The measured z-vertex distribution over the whole run period was also put into the Monte Carlo programs used for the efficiency calculations. The probability for an event to trigger was then derived from the MC simulations. Figure 5 shows the acceptance as a function of the photon energy for the different subprocesses. One can see that only a small fraction of events, namely elastic and proton diffraction channels ($17 \pm 4\%$ of the total cross section) are invisible in both tagged and non-tagged samples. The mean efficiency for tagged events is about 6 times higher than for non-tagged ones. The significant difference in the efficiencies for the 'hard' and 'soft' γp events leads to a model dependence of the acceptance and was included in the systematic error.

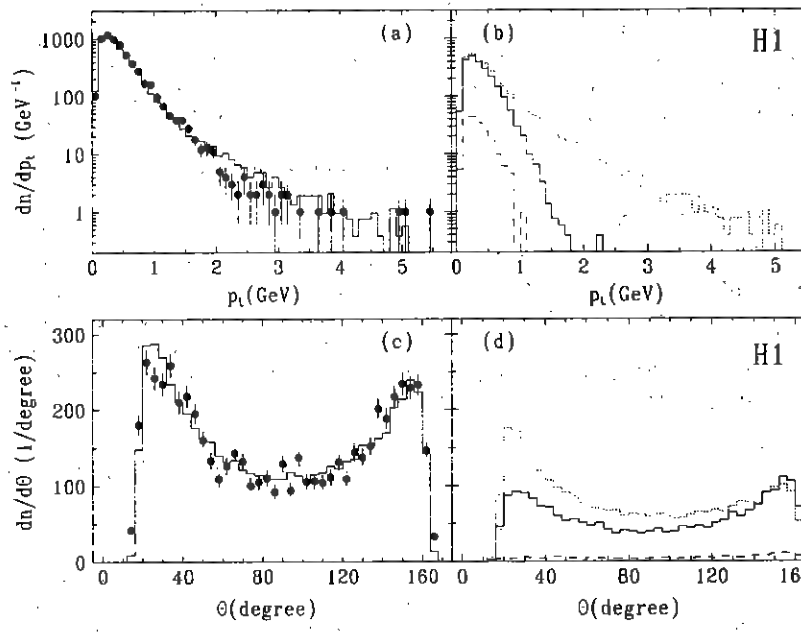

Figure 4: Inclusive transverse momentum (a) and polar angle (c) distributions of ch particles in the tagged events (points) compared to the Monte Carlo (histogram (b) and (d) the contributions of 'soft' (solid), 'hard' (dotted) and diffractive (da components are shown.

The sensitivity of the final result to the different model parameters has been st varying the most important of them within $\pm(20-30)\%$ around the standard va

- gaussian width of the transverse momentum distribution for primary hadr the fragmentation, $\sigma(p_{t,x}) = \sigma(p_{t,y}) = 350 \pm 100$ MeV/c,
- $\hat{p}_T$ cut for the hard scattering $2 \to 2$ subprocesses: $\hat{p}_T^{min} = 2.5 \pm 0.5$ GeV/c
- elastic and diffractive slopes $b_{el} = 12 \pm 3$ GeV^{-2}, $b_{sd} = 6 \pm 1.5$ GeV^{-2} [17].

It was found that 20% changes of these parameters lead to a 3% change of the efficiency for the tagged sample and to an 8% change for the non-tagged sample main contribution to the systematic error comes from the uncertainty in the compo of the total cross section.

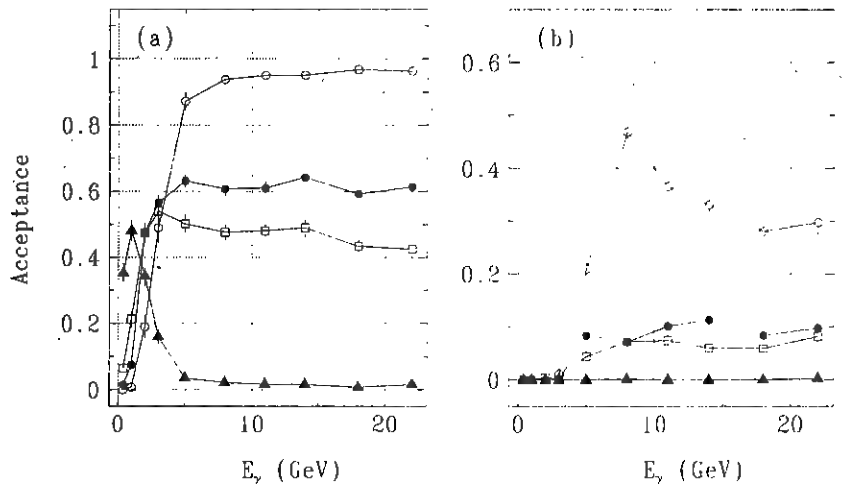

Figure 5: Acceptances for the different γp subprocesses as a function of the photon energy for the tagged (a) and non-tagged (b) events. Open circles = 'hard' processes, full circles = 'soft' processes, squares = γ-diffraction ($\gamma p \to M_x p$ and $\gamma p \to M_{x1} M_{x2}$), triangles = 'elastic' and proton diffraction.

Finally, the following result for the photon flux averaged acceptances was obtained:

$$< A > = \frac{\int_{y_{min}}^{y_{max}} A(y) Flux(y) dy}{\int_{y_{min}}^{y_{max}} Flux(y) dy} = \begin{cases} 0.274 \pm 0.026 & \text{for tagged sample} \\ 0.098 \pm 0.018 & \text{for non-tagged sample} \end{cases}$$

where y_{min}, y_{max} define the limits of the area with non-zero acceptance. An average electron tagger acceptance for the energy range $10 < E_{e'} < 19$ GeV is 0.48 ± 0.02 and is included in $< A >$ for the tagged sample.

6 Cross Section

For both data samples an average $\sigma_{tot}(\gamma p)$ was calculated by integrating the ep differential cross section (2) over the full y range while taking into account the detector acceptance $A(y)$ as described in the previous section:

$$\sigma_{tot}(\gamma p) = \frac{N_{\gamma p}}{\mathcal{L} \int_0^1 A(y) Flux(y) dy (1 + \delta_{WWA})},$$

where δ_{WWA} is a global correction to the Weizsäcker-Williams approximation, $N_{\gamma p}$ is the total number of observed photoproduction events, and $\mathcal{L}$ is the integrated luminosity $\int L dt$.

As already mentioned, the luminosity L was determined from the rate of strahlung events. After subtraction of background from the residual gas and acc for the acceptance of the system one gets

$$L = \frac{R_{tot} - (I_{tot}/I_0) R_0}{\sigma_{vis} C(\theta_x, \theta_y)}$$

where R_{tot} is the total $e\gamma$ coincidence rate and R_0 is the rate in the electron pilot I_{tot}, I_0 are the corresponding currents and σ_{vis} is the visible part of the ep cross section for the nominal beam conditions. The factor $C(\theta_x, \theta_y)$ accounts dependence of the acceptance of the luminosity system on the electron beam tilt horizontal and vertical planes. Already in this first running period the statistic in the integrated luminosity was negligible compared to the systematic error fr acceptance determination. A Monte Carlo simulation has shown that the per monitoring of the electron beam tilt with the precision of $\Delta\theta_x$, $\Delta\theta_y \approx 0.02$ achieved experimentally, guarantees an overall systematic error to be less than 7% main effect comes from the uncertainty in the acceptance, while the trigger eff and the detector calibration contribute $\sim 3\%$ to the systematic error. The error background subtraction due to the systematics in the current measurements ha checked in stand alone electron beam runs and was found to be less than 2%. A run taken for the acceptance study has proven that for an electron beam tilt ± 0.2 mrad the Monte Carlo estimate differs from the data by less than 5%. Th total luminosity error has been estimated as

$$\Delta\mathcal{L} = 0.4\%(stat.) + 7.0\%(syst.)$$

The γp total cross section defined from the tagged sample has been corrected radiative process $ep \to e'\gamma X$. The radiative corrections were calculated with the the TERAD91 program adapted to the low Q^2 domain [18]. For the actual experi conditions the following result was obtained:

$$\delta_{RC} = (2.5\ ^{+1.4}_{-2.2})\% ,$$

where $\sigma_{meas} = (1 + \delta_{RC}) \sigma_{Born}$. Thus for the tagged sample we give our measure the Born cross section at the average center of mass energy of $W_{\gamma p} = 195$ GeV the error of δ_{RC} is included in the total systematic error:

$$\sigma_{tot}(\gamma p) = 159 \pm 7(stat.) \pm 20(syst.)\ \mu\text{b}.$$

For the non-tagged sample the total γp cross section at an average $W_{\gamma p} = 18$ was found to be $\sigma_{tot}(\gamma p) = 152 \pm 10(stat.) \pm 32(syst.)\ \mu$b. The final results fo methods are summarized in the table below where the statistical and systematic are added in quadrature.

Sample	$W_{\gamma p}$[GeV]	$N_{\gamma p}$	$\mathcal{L}$ [μb^{-1}]	$< A >$	δ_{WWA} [%]	$\sigma_{\gamma p}$
tagged	195	917 ± 38	1536 ± 109	$.274 \pm .026$	-0.2 ± 0.1	159
non-tagged	183	940 ± 65	1081 ± 76	$.098 \pm .018$	-12 ± 1	152

The energy dependence of the total photoproduction cross section is shown in Figure 6 where our result from the tagged sample is compared with the ZEUS measurement [4] and with low energy data [2]. For both HERA experiments statistical and systematic errors are added in quadrature. The inner error bars show the statistical errors

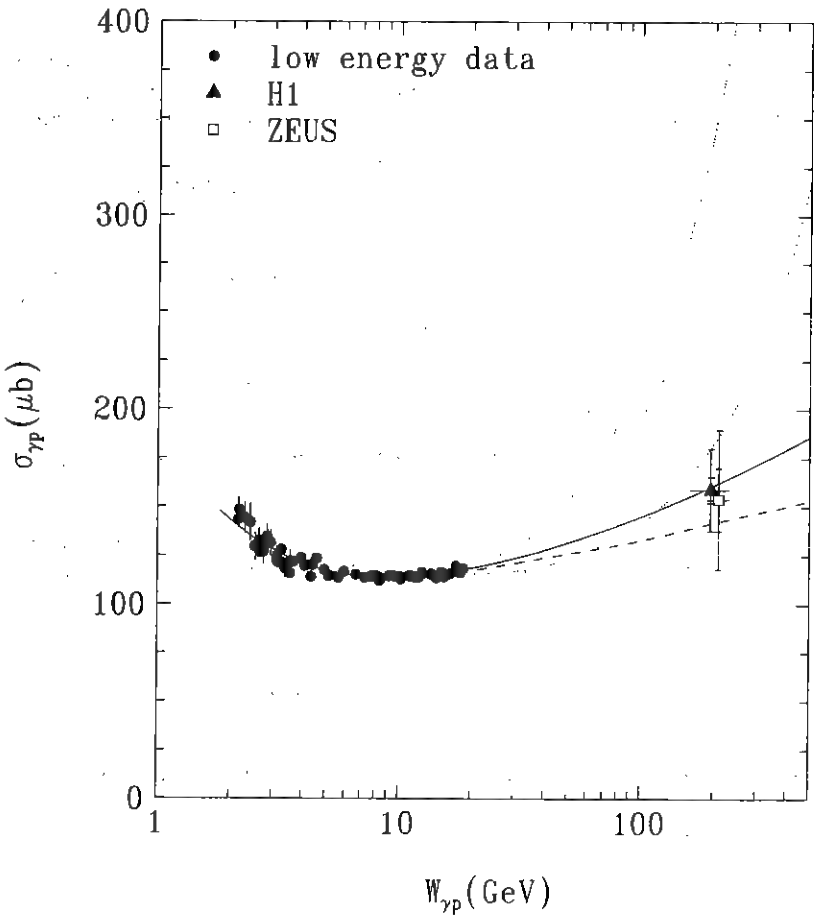

Figure 6: The total γp cross section measurements at low energies together with those measured at HERA by H1 and ZEUS. The solid curve represents a Regge based fit of low energy data [19]. The dashed curve is the prediction of ALLM parametrization [20]. The dotted lines are obtained using PYTHIA Monte Carlo with the DG parametrization of the photon structure function for $\hat{p}_T^{min} = 1.4$ GeV/c (upper line) and for $\hat{p}_T^{min} = 2.0$ GeV/c (lower line).

only. The curves represent three main categories of theoretical predictions: parar
tion of the existing data, Regge approach and QCD minijets. The phenomen
extrapolation from low energies are usually based either on the vector-meson dor
model or on the Regge model. As an example of this class the full line shows a
published fit [19]. Another Regge-type parametrization [20] based on the ana
γp and $\gamma^* p$ data is shown by the dashed line. Finally, the dotted lines are
cross section calculated by PYTHIA 5.6 using the ansatz $\sigma_{\gamma p}(s) = \sigma^{soft} + \sigma^{j}$
these calculations the KMRS B^0 [21] proton structure function and the DG [22]
structure function were used. The upper and lower curves correspond to differe
cutoffs. Minijet models [23] assuming a very small $\hat{p}_T^{min} < 1.4$ GeV/c seem to b
out.

7 Conclusions

The γp total cross section has been measured in the new energy domain off
the HERA ep collider. Two independent methods gave consistent results. Ou
surement does not support extreme minijet models predicting a strong rise of
total cross section with energy. It is in a good agreement with the Regge mo
parametrizations.

Acknowledgements

We are very grateful to the HERA machine group whose outstanding effort
this experiment possible. We acknowledge the support of the DESY computer
We appreciate the big effort of the engineers and technicians who construct
maintained the detector. We thank the funding agencies for financial support
experiment. The non-DESY members of the collaboration also want to thank the
directorate for the hospitality extended to them.

References

[1] G.A. Schuler, Proc. of the Workshop on Physics at HERA, DESY (199
A. Levy, ibid, 481; S. Levonian, ibid, 499; G. Schuler and J. Terron, CE
6415/92 (1992)

[2] S.I. Alekhin at al., *Compilation of cross sections. 4*, CERN-HERA 87-01 (1

[3] F. Eisele, *First Results from the H1 experiment at HERA*, Invited talk, Proc
26th Int. Conf. on High Energy Physics, Dallas, 1992 and DESY preprint
(1992)

[4] ZEUS Collaboration, M. Derrick et al., Phys.Lett., B293 (1992) 465.

[5] C.F. Weizsäcker, Z.Phys. 88 (1934) 612; E.J. Williams, Phys.Rev. 45 (1934